



# Simulation model for the evaluation and design of miniaturized non-resonant photoacoustic gas sensors

Jochen Huber<sup>1,2</sup>, Katrin Schmitt<sup>1</sup>, and Jürgen Wöllenstein<sup>1,2</sup>

<sup>1</sup>Fraunhofer Institute for Physical Measurement Techniques IPM, Heidenhofstr. 8, 79110 Freiburg, Germany

<sup>2</sup>Laboratory for Gas Sensors, Department of Microsystems Engineering-IMTEK, University of Freiburg, Georges-Koehler-Allee 102, 79110 Freiburg, Germany

Correspondence to: Jochen Huber (jochen.huber@ipm.fraunhofer.de)

Received: 26 April 2016 – Revised: 15 June 2016 – Accepted: 4 July 2016 – Published: 28 July 2016

**Abstract.** This publication reports the derivation and the implementation of a simulation model that describes non-resonant photoacoustic gas sensors. The photoacoustic effect is modelled in detail for the successive steps of radiation emission, stimulation of molecules, collisional relaxation processes and finally the pressure formation in a closed gas cell. The photoacoustic effect offers great potential in the development of selective, miniaturized gas sensor systems. We verify and discuss the results of our model assuming typical parameters and values in indoor CO<sub>2</sub> sensing applications. We set up a sensor system for experimental verification of the simulated data and discuss the results. The results of the simulation model are in good accordance with the experimental data and can therefore be used as a novel and efficient tool for the development of non-resonant photoacoustic gas sensor systems.

## 1 Introduction

Infrared (IR)-active gases like carbon dioxide (CO<sub>2</sub>), methane (CH<sub>4</sub>), water (H<sub>2</sub>O) or carbon monoxide (CO) can be detected very selectively using infrared spectroscopic measurement techniques. The photoacoustic spectroscopy (PAS) is widely recognized as a specific technique suitable for monitoring IR active gases in low concentrations. Especially the above-mentioned gases absorb very selectively in the mid-infrared wavelength range between 3 and 10 μm (Demtröder, 2013). Bell (1880), Tyndall (1880) and Röntgen (1881) were the first to describe the photoacoustic effect, as they observed that a beam of sunlight rapidly interrupted with a rotating slotted wheel generated sound waves directly from a solid sample. Today photoacoustic spectroscopy is used in a variety of applications, from industrial process monitoring to high precision trace gas monitoring. Good overviews of the possible applications of photoacoustic spectroscopy are given by West et al. (1983), Hodgkinson and Tatam (2013) and Bozóki et al. (2011). The operation modes of photoacoustic spectroscopic systems can be subdivided into resonant and non-resonant. Resonant cells are

mainly used in trace gas monitoring, requiring a high level of sensitivity. Here, laser sources or IR diodes can be modulated with high frequency to cause a resonant standing wave in a detection chamber. Using gas lasers, resonant photoacoustic systems have been reported to reach detection limits in the parts-per-billion (ppb) range (Sigrist, 1995; Schilt et al., 2004). However, resonant systems are rather bulky and cost-intensive. In contrast, non-resonant systems can be realized in much less space at lower component costs, making them suitable for applications requiring less sensitivity. Often broadband IR sources such as filament or planar thermal emitters are used. An advantage of broadband emitters is that all absorption lines of the gas contribute to the signal, allowing a reduction of the optical path length. A prominent application example is room climate (i.e. indoor air) monitoring, evaluating CO<sub>2</sub> as a parameter for air quality. In our study we focus on a non-resonant sensor set-up exploring its high potential for miniaturization. The mathematical description of the photoacoustic effect with its physical background has been described in literature before. For example Rosengren (1973a, b) has published theoretical models for photoacoustic sensors in general. Other publications describe sim-

ulation models for specific photoacoustic gas sensors also in resonant operation mode (Besson et al., 2006; Miklós, 2015). There is a high number of limitations for geometrical parameters in these published simulation models. Schulz (2008) and Salleras et al. (2004) have described a complex simulation model regarding a non-resonant set-up with potential for miniaturization. We discuss a simulation model for a non-resonant mode sensor, yet additionally take influences from the sensor environment into account. The focus of our simulation model is the investigation of a miniaturized, robust and low-cost photoacoustic gas sensor with several absorption chambers. Further the model should not be too complex to allow integration into a fast simulation tool. The main boundary conditions and environmental parameters are considered. The simulation model can be used as an effective tool for further sensor developments like miniaturization or specific designs for certain applications. The theoretical background of the effect is described and the mathematical derivation of the pressure signal in the detection chamber is shown. Simulation results for an exemplary set-up are discussed and compared with measurement results of an implemented sensor system. Finally the results are evaluated and the future potential is discussed.

## 2 Theoretical background

The photoacoustic effect is based on the absorption of photons. The effect is described as the process of acoustic wave generation in a sample resulting from the absorption of photons (West et al., 1983). The photoacoustic signal is generated by modulated light at a wavelength coinciding with an absorption band of the component to be measured (Bozóki et al., 2011). A major part of this energy is transformed into translational energy of the molecules (Rosengren, 1973b). This local translational energy is spread in the gas volume and can be detected as pressure wave. In photoacoustic sensors, the absorbed light is measured directly. The transformation of the energy into an acoustic signal in dependence on the gas concentration of the target gas is described in five steps as they are shown in Fig. 1:

- Emission of radiation
- Stimulation of molecules by absorption
- Gas dynamic processes
- Formation and propagation of a pressure wave
- Detection of the pressure signal

These five steps are modelled separately in the following derivation. The sensor performance and its response to system parameters are simulated in detail. Finally all mathematical models of the described steps are combined in a complete simulation model for our photoacoustic gas sensor

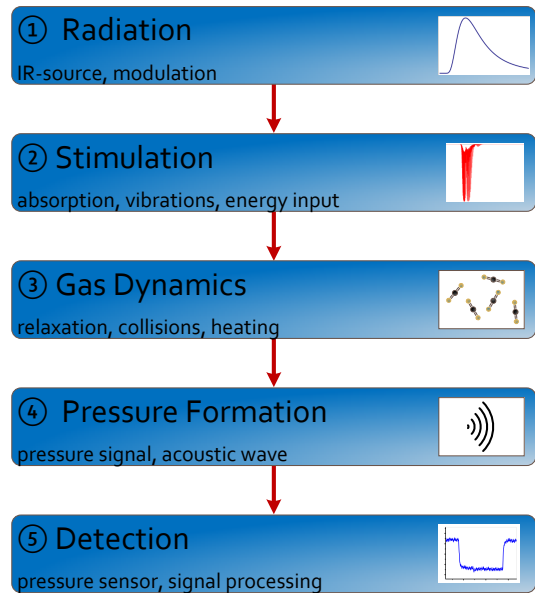


**Figure 1.** Visualization of the formation of a photoacoustic wave in five steps.

set-up. The simulation model allows prediction of the pressure signal strength in the detection chamber. The following derivation is performed for a molecular gas. The first step in Fig. 1 describes the emission of IR light by a light source. The light source has the maximum intensity  $I_0$  ( $\text{W m}^{-2}$ ). We assume a black body-like thermal emitter as a broadband IR source. The light source is modulated over time with a sinusoidal function  $\sin(\omega t)$  with angular frequency  $\omega$  ( $\text{s}^{-1}$ ). The resulting transient emitter signal can be described as

$$I(t) = \frac{I_0}{2} \cdot \sin(\omega t) + \frac{I_0}{2}. \quad (1)$$

The intensity is a quantity always greater than zero. Because of that the emitter mode function is shifted into the positive quadrant.

The emitted energy  $E(t)$  for a defined sensor set-up can be calculated with the surface area  $A$  ( $\text{m}^2$ ) of the emitter to

$$E(t) = \int_0^t I(t) \cdot A dt = \int_0^t P(t) dt. \quad (2)$$

This energy is partially converted into internal energy of the gas by molecular absorption. If a photon is absorbed by a molecule with energy level  $E_L$  ( $J$ ) (lower state), it is excited to a higher energy level  $E_H$ . The densities ( $N_H$ ,  $N_L$  ( $1 \text{ m}^{-3}$ )) of the energy levels, the excitation rate  $R$  of the molecules and the decay constant  $\tau_d$  (s) representing the average lifetime of an excited molecule are considered. The differential equation for the energy introduction can be expressed as

$$\frac{dN_H}{dt} = N_L \cdot R(t) - \frac{N_H}{\tau_d}. \quad (3)$$

The excitation rate  $R$  can be expressed using the absorption cross section  $\sigma$  and the photon flux  $\psi(t)$  ( $\text{m}^{-2} \text{s}^{-1}$ ):

$$R = \psi(t) \cdot \sigma. \quad (4)$$

The differential equation can be written as follows:

$$\frac{dN_H}{dt} = N_L \cdot \psi(t) \cdot \sigma - \frac{N_H}{\tau_d}. \quad (5)$$

The photon flux  $\psi(t)$  is the ratio of the emitted intensity and the mean energy of the excited energy level  $E_H$ :

$$\psi(t) = \frac{I(t)}{E_H}. \quad (6)$$

Assuming that the density of excited energy levels is much lower than the lower state energy density, the following simplifications can be assumed:

$$N_H \ll N_L, \quad (7)$$

$$N_0 = N_H + N_L, \quad (8)$$

$$N_L \approx N_0. \quad (9)$$

$N_0$  is the total molecular density. Now, Eq. (5) can be simplified to

$$\frac{dN_H}{dt} = N_0 \cdot \psi(t) \cdot \sigma - \frac{N_H}{\tau_d}. \quad (10)$$

The solution of Eq. (10) is the time-modulated density of excited-state molecules through absorption, concerning spontaneous decay of excited state molecules.

The term

$$N_0 \cdot \psi(t) \cdot \sigma \quad (11)$$

can be converted into an expression depending on the total emitted power  $P(t)$  ( $\text{W s}^{-1}$ ), the volume  $V$  ( $\text{m}^3$ ) and the probability of excitation  $k$  which is determined from  $\sigma$ . The result is the following relation:

$$N_0 \cdot \psi(t) \cdot \sigma = \frac{P(t)}{\varepsilon \cdot V} \cdot k \quad (12)$$

Inserting this relation into Eq. (10) results in the differential equation:

$$\frac{dN_H}{dt} = \frac{P(t)}{\varepsilon \cdot V} \cdot k - \frac{N_H}{\tau_d}. \quad (13)$$

$P_0$  is the maximum power emitted at a certain time. Analogous to Eq. (1), the time-dependent power  $P(t)$  is assumed to be a sinusoidal signal according to

$$P(t) = \frac{P_0}{2} \cdot \sin(\omega t) + \frac{P_0}{2}. \quad (14)$$

With this term for  $P(t)$ , the differential equation for the excited state density  $N_H$  has the following analytical unique solution:

$$N_H(t) = \frac{k \cdot \tau_d \cdot P_0 \cdot (1 + \tau_d^2 \cdot \omega^2 - \tau_d \cdot \omega \cdot \cos(\omega t) + \sin(\omega t))}{V \cdot \varepsilon \cdot (1 + \tau_d^2 \cdot \omega^2)}. \quad (15)$$

Knowing of the density of excited state molecules inside the measurement volume, it is possible to calculate the resulting pressure signal. The pressure is defined as

$$\Delta p = \frac{2}{3} \cdot n_H \cdot \varepsilon \quad (16)$$

with

$$n_H = N_H \cdot V. \quad (17)$$

The derivation of this relation can be found in (Hänel, 2004). To calculate pressure signal  $\Delta p$  of the excited molecules, loss mechanisms have to be taken into account. However, only pressures above the static pressure of the atmosphere  $p_{\text{atm}}$  can be measured. Thus the resulting expression is

$$\frac{dp}{dt} = \frac{2}{3} \cdot \varepsilon \cdot \frac{n_H(t)}{\tau_c} - \frac{p(t) - p_{\text{atm}}}{\tau_{\text{th}}}. \quad (18)$$

This differential equation can be analytically solved under the assumption of a sinusoidal power emission of the IR source  $P(t)$ . The unique solution is given by

$$p(t) = p_{\text{atm}} + \frac{2 \cdot k \cdot P_0 \cdot \tau_d \cdot \tau_{\text{th}}}{3 \cdot V \cdot \tau_c} \cdot \left( 1 - \frac{(\tau_d + \tau_{\text{th}}) \cdot \omega \cdot \cos(\omega t) + (\tau_d \cdot \tau_{\text{th}} \cdot \omega^2 - 1) \cdot \sin(\omega t)}{(1 + \tau_d^2 \cdot \omega^2) \cdot (1 + \tau_{\text{th}}^2 \cdot \omega^2)} \right). \quad (19)$$

The time constant  $\tau_{\text{th}}$  (s) is the thermal time constant for heat exchange between the gas and the environment.  $\tau_c$  (s) describes the time constant of the collisional relaxation process. It represents the mean time of a translation–vibration energy transition between two molecules.

## 2.1 Model description

The above-described relations are the basis for our simulation model to predict the resulting pressure sensor signal in a detection chamber of a photoacoustic gas sensor. We use a two-chamber sequential set-up for selective measurements in real time. The functional principle of the sensor can be seen in Fig. 2.

The IR source emits time modulated IR emission at a defined frequency. In case no IR active molecules are present outside the detection chamber, the light and therefore signal intensity is maximal. In turn, if IR active molecules are present in the absorption (measurement) path, they absorb a part of the IR light, leaving less optical power to enter the

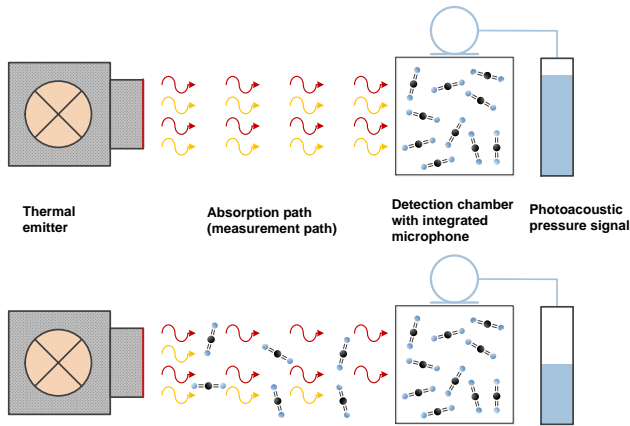


**Figure 2.** Working principle of the sensor set-up. Part of the light from the thermal emitter is absorbed in the measurement path if IR active molecules are present, leading to a decreased photoacoustic pressure signal.

detection chamber with the enclosed target gas. Due to this, a lower photoacoustic pressure signal is measured. Thus it is an indirect measurement of the gas concentration in the measurement path. To calculate the signal inside the detection chamber, a two-step absorption calculation has been considered. Furthermore IR transparent windows reduce the intensity of the IR light, which also has to be taken into account.

We use HITRAN (CFA Harvard, 2008) data to simulate the absorption  $A(\lambda)$  in the volumes (measurement path and detection chamber). A transmission spectrum for 1000 ppm CO<sub>2</sub> is displayed in Fig. 3. We assume a grey body emitter profile  $F(\lambda)$  with a defined temperature and an emission factor  $a < 1$  as IR source. We multiply the imported discrete transmission data set  $(1 - A_1(\lambda))$  for the measurement path by the corresponding discrete values of the transmission profiles of the two IR transparent windows  $W_i(\lambda)$  and finally by the absorption data  $A_2(\lambda)$  in the detection chamber to obtain

$$A_{\text{final}}(\lambda) = W_1(\lambda) \cdot (1 - A_1(\lambda)) \cdot W_2(\lambda) \cdot A_2(\lambda). \quad (20)$$

Finally the resulting absorbed energy is calculated as numerical integration of the final absorption data with the grey body emitter profile:

$$P_0 = \int A_{\text{final}}(\lambda) \cdot F(\lambda) d\lambda. \quad (21)$$

$P_0$  is modulated with a sinusoidal curve as described in Eq. (14). The pressure signal is then calculated as described in Eq. (19).

## 2.2 Input parameters

To calculate the pressure signal in the detection chamber, discrete parameter values describing the sensor system are chosen. The simulation model is implemented in MATLAB

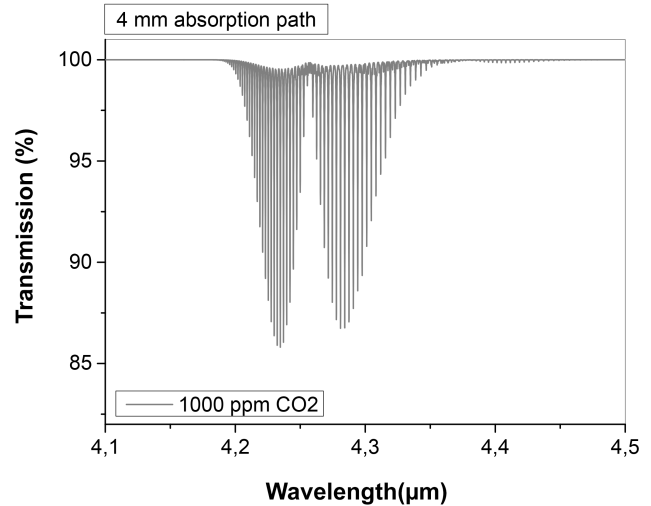


**Figure 3.** Transmission spectrum of 1000 ppm CO<sub>2</sub> in N<sub>2</sub> at 4 mm absorption length under standard conditions (296 K, 1 atm).

and a set of input parameters was defined. Table 1 gives the parameters with their units and values as used in the simulation. With the above-listed parameters a number of simulations have been performed, varying different influencing parameters like modulation frequency, input power, gas concentration and chamber volume. The parameters were specified for our miniaturized sensor system in non-resonant operation mode, which was also experimentally realized to perform measurements. The target application of the developed system is the measurement of indoor air quality (0–5000 ppm CO<sub>2</sub>) in sufficient resolution ( $\sim 200$  ppm). The environmental parameters have been chosen according to an operation environment at standard conditions ( $T = 298$  K,  $p = 1013$  mbar). The decay constants are estimated for a system made of aluminium. All parameters are assessed for the typical indoor air condition application with ideal gases and the main absorption region of CO<sub>2</sub> at about 4.25  $\mu\text{m}$ . Figure 4 shows the transient simulated pressure signal compared to the profile of the emitted modulated light. A time delay between the modulated light signal and the pressure signal can be observed. A constant concentration of 300 ppm CO<sub>2</sub> was assumed.

Figure 5 shows a simulation of the influence of the modulation frequency on the amplitude of the signal for 300 ppm CO<sub>2</sub> present in the measurement path. A lower frequency results in a higher amplitude signal, which can be explained as follows: in a longer on-phase of the emitter, more molecules can be excited. This results in a higher relaxation ratio after switching off the light source. This leads to a higher pressure difference between on- and off-phase of the emitter. The simulation model estimates a long lifetime of the excited molecules. If the modulation frequency is low, the warm-up time of the emitter is long compared to the mean lifetime of the excited molecules, i.e. the molecules re-

**Table 1.** Parameters used in the simulation model.

Parameter	Symbol	Value	Unit
Emission factor	$a$	0.8	–
Emitter area	$A$	$2.2 \times 2.2$	$\text{mm}^2$
Emitter temperature	$T_E$	850	K
Absorption length measurement path	$s$	5	mm
Absorption length detection chamber	$d$	2.2	mm
Environmental temperature	$T$	296	K
Static pressure	$P_{\text{atm}}$	1013.25	mbar
Molecular density	$N_0$	$2.687 \times 10^{25}$	$\text{m}^{-3}$
Frequency	$f$	13	Hz
Excitation probability	$k$	1	–
Mean energy of an absorbed photon	$\varepsilon$	$4.654 \times 10^{-20}$	J
Decay constant: lifetime excited state (spontaneous relaxation)	$\tau_d$	$1 \times 10^{-5}$	s
Decay constant: collisional relaxation	$\tau_c$	$1 \times 10^{-4}$	s
Decay constant: thermal heat losses	$\tau_{\text{th}}$	$1 \times 10^{-1}$	s
Volume of detection chamber	$V$	$1.9 \times 10^{-7}$	$\text{m}^3$

lax during a long on-phase of the emitter. As a consequence the maximum density of the excited state is not reached as estimated in the simulation. That means that there is an optimum frequency for maximum pressure signal during an emitter activation phase. Therefore we have to find the trade-off between measurement rate (high frequencies) and amplitude level (low frequencies). For the variation of the parameters other than modulation frequency, we have defined 13 Hz as a constant emitter modulation frequency for the operation of the system. Also, for the measurements we use a modulation frequency of 13 Hz.

A simulation for our experimental set-up (cf. Sect. 3) and the target gas  $\text{CO}_2$  is depicted in Fig. 6. The concentration range used in the simulation is 0 to 100 000 ppm  $\text{CO}_2$  (10 %). The signal decays exponentially with concentration as we would expect from the Beer–Lambert law. Compared to NDIR sensors, we do not observe a saturation of the sensing signal, because all absorption lines of the target gas are contained in the signal. Especially at higher concentrations of the target gas, the main absorption lines are already in saturation and weaker side lines increasingly dominate the signal, i.e. the sensitivity. Therefore the measurement range of a PAS sensor can be easily adapted to the application. For example, for room climate monitoring, a measurement range up to 5000 ppm  $\text{CO}_2$  is optimal. In this range the sensor is more sensitive due to a higher gradient of the sensor response

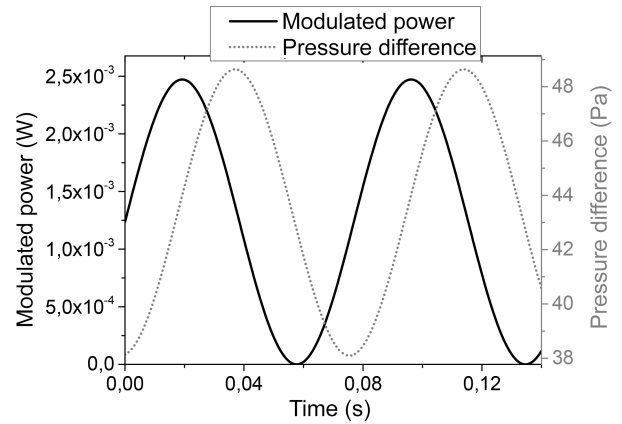


**Figure 4.** Phase shift between the modulation signal and the resulting pressure wave in the detection chamber.

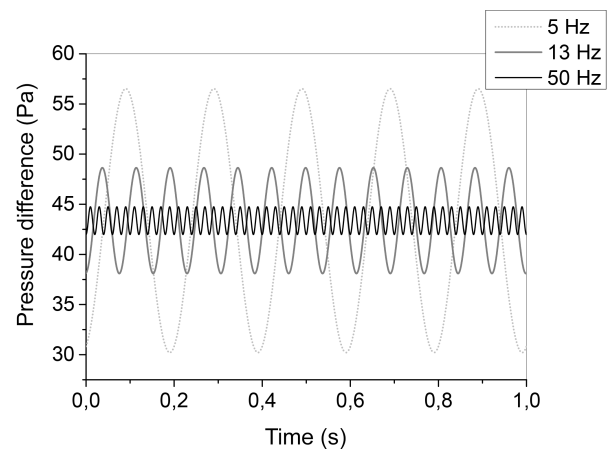


**Figure 5.** Amplitude (pressure difference) in dependence of the modulation frequency of the PAS system.

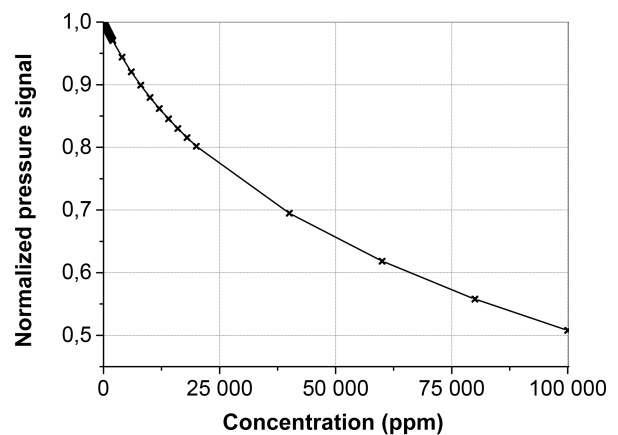


**Figure 6.** Simulated sensor response for  $\text{CO}_2$  concentrations up to 100 000 ppm in the measurement path. Parameters are chosen as listed in Table 1.

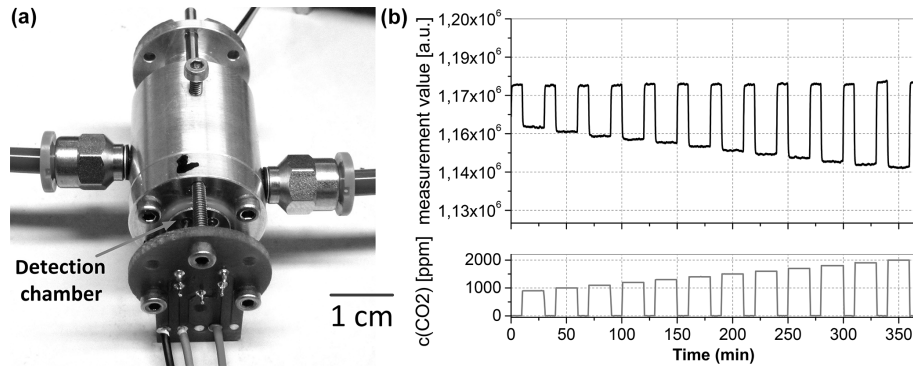


**Figure 7.** (a) Measurement set-up with detection chamber in a TO housing. (b) Concentration measurement in the range from 900 to 2000 ppm CO<sub>2</sub> in N<sub>2</sub> in steps of 100 ppm.

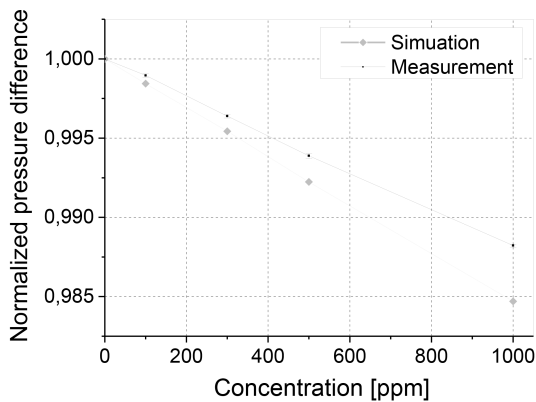


**Figure 8.** Comparison of measurement and simulation results for our PAS sensor.

curve. Also, the sensor response in this measurement range can be approximated as linear. This fact makes the calibration of a sensor less complex and a linear function can be implemented.

### 3 Experimental results and discussion

To verify the simulation results, we set up a miniaturized PAS sensor for experimental testing. Figure 7a shows a photograph of the sensor set-up that fits to the parameters which have been chosen for the simulations. We use a commercially available MEMS emitter as an IR source (IR66, Hawkeye Technologies, Milford, USA). The detection chamber is realized in a TO housing with an integrated MEMS microphone as detector (SMM310, Infineon, Munich, Germany). The detection chamber has been described in detail earlier (Huber et al., 2014). The sensor housing made of aluminium allows variable absorption path lengths to characterize the detection unit.

We have performed measurements with CO<sub>2</sub> in N<sub>2</sub> at a calibrated gas test stand. Figure 7b depicts an exemplary measurement result. The measurement was performed in the

concentration range between 900 and 2000 ppm steps of 100 ppm. The sensitivity is better than 100 ppm this range, because the standard deviation of 20 measurements is smaller than the difference of the sensor value between the 100 ppm steps. The sensor output is an alternating signal, evaluated with a microcontroller board with a digitally implemented lock-in amplifier. The output is a value that is directly related to the gas concentration. To compare the experimental results with the simulated values, the analogue signal processing and the digital data algorithms are also added to the simulation model in MATLAB. The output values are normalized to the value of 0 ppm CO<sub>2</sub> as maximum output value. The comparison of the experimental and simulation results is shown in Fig. 8. The pressure difference falls with increasing gas concentration. The measurement was repeated 13 times. The maximum standard deviation is smaller than 0.012 % of the absolute measurement value. The sensor response can be approximated with a linear function in a small concentration range (here: 0–1000 ppm). For higher concentrations the sensor response is nonlinear as it can be seen in the simulation in Fig. 6. The slope of the simulated curve is 22.6 % higher than the slope of the experimental curve. A possible reason for this could be effects the absorption path not reflected in the simulation. In reality reflections and other non-ideal effects occur, leading to a variety of optical paths in the sensor. These overlap, a phenomenon called “effective absorption path length”. Our simulation model as it is now can be used for the prediction of photoacoustic gas sensor set-ups that are ideal, yet a detailed investigation of the influence of the effective absorption path has to be done in future. Another possible reason for the difference between simulation and measurement sensitivity is probably the environmental temperature. We assume a mean temperature of 25 °C for the computation of the absorption lines. The system is affected by heat energy from the thermal emitter which results in higher temperature of the system. This leads to a modified absorption line strength which is not considered in the simulation model. Here the real temperature needs to be considered in future.

## 4 Conclusions

We report the detailed derivation of a simulation model describing a two-chamber photoacoustic set-up in non-resonant operation mode. All sensor boundary conditions are considered. The system prediction is possible with minor deviation to the measured sensor values. The described model shows the suitability as effective and fast development tool allowing varying boundary conditions for design considerations of non-resonant photoacoustic gas sensors. Our experimental set-up provides a high potential for low-cost and therefore mass-market applications, because the simulations indicate that the reduction of the detection chamber volume results in a higher photoacoustic signal with the same cross section of the opening for light entry. Our described simulation model is restricted in some aspects because we assume an ideal behaviour of the investigated gases. A further miniaturization is possibly limited because of non-ideal effects which are not considered by the simulation model yet. For example, the simulation tool will always indicate a volume reduction as signal increase. We assume that if the chamber dimensions are close to the mean free path lengths of the molecules, there will be no signal detected by the microphone. In this scenario the ratio of surface to volume is too large. If the number of molecules adherent at the walls of the chamber is higher than the number of molecules in free movement, the pressure signal decreases strongly. This limitation has to be investigated experimentally. Another aspect that is not considered in the simulation model is a possible thermal crosstalk between the detector and the emitter if the distance between these components becomes too small. This effect results in a very high false signal due to the heat flow. Altogether we see the described simulation model as effective tool for the analysis and development of miniaturized photoacoustic gas sensors. The sensor concept shows a great miniaturization potential and enables selective gas measurements. Another interesting aspect of this set-up is that we use mass-market components, such as a MEMS microphone as it is used in mobile phones. Our photoacoustic sensor, here optimized for CO<sub>2</sub> detection, can be easily adapted to other IR active gases, e.g. CH<sub>4</sub>, CO or H<sub>2</sub>O.

## 5 Data availability

The data presented in this paper are available on request from the corresponding author.

## Competing interests

The authors declare that they have no conflict of interest.

**Acknowledgements.** We gratefully acknowledge financial support from the European Union under the framework of the ENIAC-JU ESEE project (<http://www.eniac-erg.org>) under

grant agreement no. 324284 and from the national authorities of Germany, the Netherlands, Finland, France and Spain. The research leading to these results has received funding from the Federal Ministry of Education and Research under grant agreement no. 16ES0042.

Edited by: B. Jakoby

Reviewed by: two anonymous referees

## References

- Bell, A. G.: On the production and reproduction of sound by light, *Am. J. Sci.*, 118, 305–324, 1880.
- Besson, J. P., Schilt, S., and Thévenaz, L.: Sub-ppm multi-gas photoacoustic sensor, *Spectrochim. Acta A*, 63, 899–904, 2006.
- Bozóki, Z., Pogany, A., and Szabo, G.: Photoacoustic instruments for practical applications: present, potentials, and future challenges, *Appl. Spectrosc. Rev.*, 46, 1–37, 2011.
- CFA Harvard, HITRAN spectral database, available at: <https://www.cfa.harvard.edu/hitran/> (last access: 21 July 2016), 2008.
- Demtröder, W.: *Laser spectroscopy: basic concepts and instrumentation*, Springer Science and Business Media, Berlin Heidelberg, Germany, 2013.
- Hänel, D.: *Molekulare Gasdynamik: Einführung in die kinetische Theorie der Gase und Lattice-Boltzmann-Methoden*, Springer-Verlag, Berlin Heidelberg, Germany, 2004.
- Hodgkinson, J. and Tatam, R. P.: *Optical gas sensing: a review*, *Measurement Science and Technology*, 24, 012004, 2013.
- Huber, J., Ambs, A., Rademacher, S., and Wöllenstein, J.: A Selective, Miniaturized, Low-cost Detection Element for a Photoacoustic CO<sub>2</sub> Sensor for Room Climate Monitoring, *Procedia Engineering*, 87, 1168–1171, 2014.
- Miklós, A.: Acoustic Aspects of Photoacoustic Signal Generation and Detection in Gases, *Int. J. Thermophys.*, 36, 2285–2317, 2015.
- Röntgen, W. C.: On tones produced by the intermittent irradiation of a gas, 1881.
- Rosengren, L. G.: A new theoretical model of the opto-acoustic gas concentration detector, *Infrared Phys.*, 13, 109–121, 1973a.
- Rosengren, L. G.: An opto-thermal gas concentration detector. *Infrared Phys.*, 13, 173–182, 1973b.
- Salleras, M., Schulz, O., Samitier, J., Marco, S., and Müller, G.: Investigations on the dynamic thermal behaviour of miniaturized photoacoustic gas detectors, *Cell*, 2710.229, 913, 2004.
- Schilt, S., Thévenaz, L., Niklès, M., Emmenegger, L., and Hügli, C.: Ammonia monitoring at trace level using photoacoustic spectroscopy in industrial and environmental applications, *Spectrochim. Acta A*, 60, 3259–3268, 2004.
- Schulz, O.: *Bestimmung physikalischer und technischer Randbedingungen zur Umsetzung eines photoakustischen Gassensors in der Mikrosystemtechnik*, Univ.-Verlag, TU Ilmenau, Universitätsbibliothek, Ilmenau, Germany, 2008.
- Sigrist, M. W.: Trace gas monitoring by laser-photoacoustic spectroscopy, *Infrared Phys. Techn.*, 36, 415–425, 1995.
- Tyndall, J.: Action of an intermittent beam of radiant heat upon gaseous matter, *P. R. Soc. London*, 31, 307–317, 1880.
- West, G. A., Barrett, J. J., Siebert, D. R., and Reddy, K. V.: Photoacoustic spectroscopy, *Rev. Sci. Instrum.*, 54, 797–817, 1983.